# Heavy meson photoproduction in peripheral *AA* collisions

M. B. Gay Ducati and S. Martins

*High Energy Physics Phenomenology Group, GFPAE IF-UFRGS Caixa Postal 15051, CEP 91501-970, Porto Alegre, Rio Grande do Sul, Brazil*

(Received 27 April 2018; published 19 June 2018)

The exclusive photoproduction of the heavy vector mesons $\psi$ and Y is investigated in peripheral Pb-Pb collisions for the energies available at the LHC, $\sqrt{s} = 2.76$ TeV and $\sqrt{s} = 5.02$ TeV. To evaluate the robustness of the light-cone color dipole formalism, previously tested in the ultraperipheral regime, the rapidity distribution and the nuclear modification factor ($R_{AA}$) are calculated for the three centrality classes: 30%–50%, 50%–70%, and 70%–90%. The ultraperipheral to peripheral regime transition was carried out by sophisticating the photon flux description and the photonuclear cross section, taking into account the effective interaction area. In our calculations, three scenarios were considered: (scenario 1) the direct application of the usual photon flux and of the photonuclear cross section with no relevant change in relation to the ultraperipheral collision (UPCs), (scenario 2) the application of an effective photon flux keeping the photonuclear cross section unchanged, and (scenario 3) also considering an effective photonuclear cross section. The results obtained with the three different scenarios were compared with the ALICE measurements, showing a better agreement with the data (only $J/\psi$ at the moment) in the more complete approach (scenario 3), mainly in the more central regions (30%–50% and 50%–70%) where the uncertainty is smaller.

DOI: 10.1103/PhysRevD.97.116013

## I. INTRODUCTION

One of the main contributions of HERA was the discovery of diffractive events, characterized by large rapidity gaps ($\eta \gtrsim 4$) with absence of hadronic activity, where one or both hadrons emerge intact in the final state, representing a relevant fraction of deep inelastic scattering [1]. Soft diffraction events contribute with (~20%) of the total inelastic proton-proton cross section and therefore must be taken into account in order to keep the background of many processes in the LHC [2,3] under control. The hard diffractive processes, responsible for the production of the states with high mass, or high $p_T$ (for example, $Q\bar{Q}$, jets, W, and Z), can be calculated from perturbative QCD. The presence of a hard scale allows us to obtain more information about the diffractive (or generalized) particle distribution functions, which describe not only the particle density but also the correlation between them [4]. In addition, the perturbative treatment also opens a way to test new ideas on the mechanism of exchange of two or more gluons in a singlet color state, usually treated as Pomeron [5].

An interesting type of diffractive process is the exclusive photoproduction of the vector mesons, in which the collision of two hadrons produces a vector meson, keeping intact the initial hadrons. This mechanism is dominant in the ultraperipheral regime, and the cross section is factorized in two terms: a quasireal photon flux, created from one of the incoming hadrons, and the photoproduction cross section, which characterizes the interaction of the photons with the target hadron. The exclusive photoproduction has been investigated in several works [6–12]. In one of our last contributions to the subject [6], we calculated the rapidity distribution for the production of Y states in Pb-Pb collisions at energies $\sqrt{s} = 2.76$ TeV and $\sqrt{s} = 5.02$ TeV. In that case, the light-cone color dipole formalism was used [13], including the partonic saturation and the nuclear shadowing effects [14–17]. This time, we are interested in testing the robustness of the dipole color formalism in the peripheral regime. In this region, the ALICE and STAR Collaborations measured an excess in the $J/\psi$ production in small $p_T$ [18,19], which could be the product of exclusive photoproduction. There are very few studies dealing with this production mechanism in the peripheral collisions regime [20–23]. In Ref. [21], which also motivates the present study, this issue is treated by modifying one of the components of the cross section, the photon flux. However, no change is made in the photoproduction cross section in relation to the ultraperipheral case. In our first paper related to the subject [20], we calculated the rapidity distribution of the $J/\psi$ with an effective photon flux constructed in terms of the usual photon flux. An effective b-dependent interaction area was

*Published by the American Physical Society under the terms of the Creative Commons Attribution 4.0 International license. Further distribution of this work must maintain attribution to the author(s) and the published article's title, journal citation, and DOI. Funded by SCOAP³.*

considered instead of a constant value $\pi R_A^2$ adopted in Ref. [21]. Here, these previous calculations are refined by applying a relevant modification also in the photoproduction cross section, following the geometrical formalism adopted in the construction of the effective photon flux. In relation to the last work, we include a new centrality class (30%–50%) as well as another dipole model, the model proposed by Iancu, Itakura and Munier (IIM model) [24]. We also enlarge the number of states under analysis, calculating the rapidity distribution for the mesons $\psi(2S)$ and $\Upsilon(1S, 2S, 3S)$ to produce a more comprehensive analysis. The main goal of this work is to evaluate the behavior of the nuclear modification factor in three different approaches: (scenario 1) direct application of the usual photon flux and of the photonuclear cross section without any modification in relation to UPCs, (scenario 2) altering only in the photon flux, and (scenario 3) modifying the photon flux and in the photonuclear cross section.

## II. EXPERIMENTAL APPROACH

The ALICE and STAR Collaborations measured the peripheral hadroproduction of the $J/\psi$ in AA collisions, revealing an excess in the production of this meson in the small transverse momentum ($p_T < 0.3$ GeV/c) at forward ($2.5 < y < 4.0$) and midrapidity ($|y| < 1$), respectively. In the ALICE paper [18], the average rapidity distribution and the nuclear modification factor $R_{AA}$ for Pb-Pb collisions were explored in the 30%–50%, 50%–70%, and 70%–90% centrality classes at $\sqrt{s} = 2.76$ TeV, Fig. 1. In addition, in the STAR paper [19], the $J/\psi$ invariant yield and $J/\psi R_{AA}$ were measured as a function of $p_T$ for 20%–40%, 40%–60%. and 60%–80% centrality classes at $\sqrt{s} = 200$ GeV

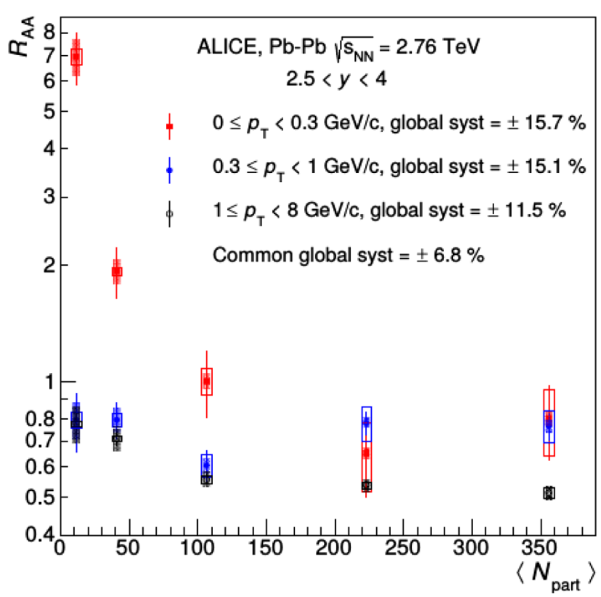


FIG. 1. $R_{AA}$ for $J/\psi$ production as a function of the average number of participating nucleons $\langle N_{\rm part}\rangle$. Figure extracted from Ref. [18].

(Au-Au) and $\sqrt{s} = 1.93$ GeV (U-U). In this work, the main goal is to test the robustness of the color dipole formalism in the same energy limit used in our previous works ($\sqrt{s} = 2.76$ TeV and $\sqrt{s} = 5.02$ TeV) to describe the rapidity distribution and $R_{AA}$. Thus, the results produced in this work will be compared with ALICE data. In a further study focused on $p_T$ dependence, data from both experiments should be considered.

To estimate the $R_{AA}$ values, we adopt the expression developed in Ref. [25],

$$R_{AA}^{hJ/\psi} = \frac{N_{AA}^{J/\psi}}{BR_{J/\psi\to l^+l^-}\cdot N_{\rm events}\cdot (A\times\varepsilon)_{AA}^{J/\psi}\cdot\langle T_{AA}\rangle\cdot\sigma_{pp}^{hJ/\psi}}, \tag{1}$$

where $N_{AA}^{J/\psi}$ represents the measured number of the $J/\psi$ ($N_{AA}^{J/\psi}$). This number was then corrected for the acceptance times efficiency $(\mathcal{A}\times\varepsilon)_{AA}^{J/\psi} \sim 11.31\%$, taking into account that photoproduced $J/\psi$ are expected to be transversally polarized, for the branching ratio $\mathrm{BR}_{J/\psi\to\mu^+\mu^-} = 5.96\%$, normalized to the number of equivalent Minimum Bias events $N_{\rm events} \simeq 10.6\times 10^7$ (calculated from Ref. [25]), for the average nuclear overlap function ($\langle T_{AA}\rangle$), the values of which depend on the centrality class and can be calculated from the Table I of Ref. [26]. In the case of the classes (30%–50%, 50%–70%, and 70%–90%), we obtained the values 3.84, 0.954, and 0.17 mb$^{-1}$, respectively. At last, the result is normalized by the proton-proton inclusive $J/\psi$ production cross section ($\sigma_{pp}^{hJ/\psi}$), which is calculated using the parametrization suggested in Ref. [18], in which

$$\frac{d^2\sigma_{pp}^{hJ/\psi}}{dp_T dy} = \frac{c\cdot\sigma_{J/\psi}\cdot p_T}{1.5\cdot\langle p_T\rangle^2}\left(1 + a^2\left(\frac{p_T}{\langle p_T\rangle}\right)^2\right)^{-n} \tag{2}$$

with

$$a = \frac{\Gamma(3/2)\Gamma(n-3/2)}{\Gamma(n-1)} \qquad c = 2a^2(n-1).$$

The values of the free parameters $\sigma_{J/\psi}$, $\langle p_T\rangle$, and $n$ are obtained from the fit of Eq. (2) with the ALICE data at large $p_T$ [27]. This procedure results in $\sigma_{J/\psi} = 3.31$, $\langle p_T\rangle = 2.369$, and $n = 4.76$. Applying these values in (2) and taking the integral in the kinematical regions of interest, $p_T < 0.3$ GeV and $2.0 < y < 4.5$, we obtain $\sigma_{pp}^{hJ/\psi} = 0.0514\ \mu$b.

In the ALICE measurement, both production mechanisms (hadro and photo) are considered, with no separation of each contribution by the detector. Theoretically, the number of the $J/\psi$ events should be separated in two terms:

$$N_{AA}^{J/\psi} = \underbrace{N_{AA}^{hJ/\psi}}_{\text{hadro}} + \underbrace{N_{AA}^{\gamma J/\psi}}_{\text{photo}}. \tag{3}$$

For the hadro component, the $J/\psi$ hadroproduction was not directly calculated but estimated from an analyses performed on the ALICE data, as shown in Fig. 1. Taking the centrality 70%–90%, for example, the $R_{AA}$ measured value in the region $p_T < 0.3$ GeV is 7, while in the range $1.0 < p_T < 8.0$, it is approximately 0.8. The $R_{AA}$ for $p_T > 1$ GeV gives a good approximation for the hadronic production of the $J/\psi$, and assuming that this contribution stays the same in the $p_T < 0.3$ region, it is possible to calculate the proportion between the hadro and photo contributions. Although the $R_{AA}^{hJ/\psi}$ data were obtained from a parametrization like Woods-Saxon, with $p_T$ dependence [18], the rough parametrizations $R_{AA}^{hJ/\psi}(p_T < 0.3\,\mathrm{GeV/c}) = R_{AA}^{hJ/\psi}(1 < p_T < 8\,\mathrm{GeV/c})$ and $R_{AA}^{hJ/\psi}(p_T < 0.3\ \mathrm{GeV/c}) = 1$, as discussed in Ref. [18], reaffirm the presence of the excess of $J/\psi$ compatible with the results reported in the experimental paper. Thus, the hypothesis considered here produces $0.8/7 \sim 0.11$ for the 70%–90% centrality class. Repeating the same procedure for the other centrality classes, 30%–50% and 50%–70%, it gives

$$(R_{AA}^{hJ/\psi})^{30\text{–}50} \sim 0.56(R_{AA}^{\gamma J/\psi})^{30\text{–}50}$$
$$(R_{AA}^{hJ/\psi})^{50\text{–}70} \sim 0.36(R_{AA}^{\gamma J/\psi})^{50\text{–}70}$$
$$(R_{AA}^{hJ/\psi})^{70\text{–}90} \sim 0.11(R_{AA}^{\gamma J/\psi})^{70\text{–}90}$$

such that

$$N_{AA}^{J/\psi} = \begin{cases} 2.27 N_{AA}^{\gamma J/\psi} & \text{for 30\%–50\%} \\ 1.56 N_{AA}^{\gamma J/\psi} & \text{for 50\%–70\%} \\ 1.12 N_{AA}^{\gamma J/\psi} & \text{for 70\%–90\%.} \end{cases}$$

Comparing the central values of the excess of $J/\psi$ with the average rapidity distribution, both shown in Table I of Ref. [18], we can infer the approximate relation $N_{AA}^{\gamma J/\psi} \sim 0.86 \times 10^6 \frac{d\sigma_{J/\psi}^{\gamma}}{dy}$, which is valid for the three centrality classes of interest. Then, the estimation of the $N_{AA}^{J/\psi}$ consists in the calculation of the average rapidity distribution, which is estimated from the integration in the range $2.5 < y < 4.0$, as

$$\left.\frac{d\sigma_{J/\psi}^{\gamma}}{dy}\right|_{2.5<y<4.0} = \frac{\int \frac{d\sigma_{J/\psi}^{\gamma}}{dy} dy}{\Delta y}. \tag{4}$$

The rapidity distribution is calculated in this work by employing the photon flux and the color dipole formalism, which are detailed in the next section.

## III. THEORETICAL FRAMEWORK

In the ultrarelativistic limit, the exclusive nuclear photoproduction cross section of the vector meson $V$ can be written as the product of a quasireal photon flux, which is produced from one of the nuclei, and the photonuclear cross section that corresponds to the photon-nuclei interaction $\gamma A \to V + A$ [28]. Considering that the photon flux carries the dependence with the impact parameter of the collision $b$, the differential cross section in the rapidity $y$ and in the impact parameter $b$ can be defined by [21]

$$\frac{d^3\sigma_{AA\to AAV}}{d^2b dy} = \omega N(\omega, b)\sigma_{\gamma A\to VA} + (y \to -y), \tag{5}$$

where $\omega = \frac{1}{2} M_V \exp(y)$ is the photon energy and $M_V$ is the meson mass.

The photon espectra, $N(\omega, b)$, are directly connected with the electromagnetic distribution of the emitting nucleus and are described by the nuclear form factor $F(k^2)$, which is the Fourier transform of the nuclear density profile. To ensure the dependence of the photon flux on the form factor, the generic formula presented in Ref. [29] is used,

$$N(\omega, b) = \frac{Z^2\alpha_{\mathrm{QED}}}{\pi^2\omega}\left|\int_0^\infty dk_\perp k_\perp^2 \frac{F(k^2)}{k^2} J_1(bk_\perp)\right|^2, \tag{6}$$

where $Z$ is the nuclear charge, $\gamma = \sqrt{s_{NN}}/(2m_{\mathrm{proton}})$ is the Lorentz factor, $k_\perp$ is the transverse momentum of the photon, and $k^2 = (\omega/\gamma)^2 + k_\perp^2$. For a heavy nucleus such as Au or Pb, the Fermi distribution with two parameters (sometimes called Woods-Saxon) is more suitable. However, to obtain the analytic result of the form factor from this distribution is unlikely, requiring the adoption of the approximation shown in Refs. [30,31], in which the Woods-Saxon distribution is rewritten as a hard sphere, with radius $R_A$, convoluted with a Yukawa potential with range $a = 7$ fm. The Fourier transform of this convolution is the product of the individual transformation as

$$F(k) = \frac{4\pi\rho_0}{Ak^3}[\sin(kR_A) - kR_A\cos(kR_A)]\left[\frac{1}{1 + a^2k^2}\right], \tag{7}$$

where $A$ is the mass number of the nuclei and $\rho_0 = 0.1385\ \mathrm{fm}^{-3}$ for Pb.

In Eq. (5), the $\sigma_{\gamma A\to VA}$ is the coherent photonuclear cross section, which characterizes the photon nuclei. In accordance with Ref. [32], the cross section for the photoproduction of a vector meson V on H (H ≡ p, A) can be factorized in two components: the forward scattering amplitude ($d\sigma/dt|_{t=0}$), which carries the dynamical information of the process, and the form factor, $F(t)$, which is, in general, dependent on the spatial characteristics of the target. This factorization has been commonly used in the

literature as can be seen in Refs. [21,32,33], in which the forward scattering amplitude was characterized, respectively, by the vector meson dominance, perturbative QCD, and color dipole formalisms. Thus, the coherent photonuclear cross section is defined as

$$\sigma_{(\gamma A\to VA)} = \frac{|\mathrm{Im}A(x,t=0)|^2}{16\pi}(1+\beta^2)R_g^2\int_{t_{\min}}^{\infty}|F(t)|^2dt. \quad (8)$$

The parameter $\beta = \mathrm{Re}A/\mathrm{Im}A$ restores the real contribution of the scattering amplitude and is usually defined as [34]

$$\beta = \tan\left(\frac{\pi\lambda\mathrm{eff}}{2}\right), \quad \text{where } \lambda_{\mathrm{eff}} = \frac{\partial\ln[\mathrm{Im}A(x,t=0)]}{\partial\ln s}.$$

Another important parameter, $R_g^2(\lambda_{\mathrm{eff}})$, is necessary for heavy mesons as $J/\psi$ and corresponds to the ratio of off-forward to forward gluon distribution (skewedness effect), being defined by [35]

$$R_g^2(\lambda_{\mathrm{eff}}) = \frac{2^{2\lambda_{\mathrm{eff}}+3}}{\sqrt{\pi}}\frac{\Gamma(\lambda_{\mathrm{eff}}+\frac{5}{2})}{\Gamma(\lambda_{\mathrm{eff}}+4)}$$

The function $F(t)$ is the same nuclear form factor shown in (7), which is integrated from $t_{\min} = (M_V^2/2\omega\gamma)^2$.

At last, the amplitude $|\mathrm{Im}A(x,t=0)|$ represents the imaginary part of the interaction amplitude for the $\gamma A \to V + A$ process. Based on the good results obtained in the last works [6–8], we describe the amplitude $\mathrm{Im}A(x,t=0)$ in the color dipole formalism, in which the photon-nuclei scattering can be seen as a sequence of the following subprocesses: (i) the photon fluctuating into a quark-antiquark pair (the dipole), (ii) the dipole-target interaction, and (iii) the recombination of the $q\bar{q}$ into a vector meson. In the quantum mechanical picture of diffraction developed by Good and Walker [36], the amplitude of this sequence of steps is written in the dipole formalism as

$$\mathrm{Im}A(x,t=0) = \int d^2r\int\frac{dz}{4\pi}(\psi_V^*\psi_\gamma)_T\sigma_{\mathrm{dip}}^{\mathrm{nucleus}}(x,r), \quad (9)$$

where the variables $z$ and $r$ are the longitudinal momentum fraction carried by the quark and the transverse color dipole size, respectively. Equation (9) is safely applicable in the low-$x$ limit, in which the transverse size of the pair $q\bar{q}$ is frozen during the interaction with the target, ensuring the applicability of the dipole formalism. It is not formally defined where the low-$x$ limit starts, and in this work, we extend the formalism up to $y = 4$ ($x \sim 0.06$ for $J/\psi$), which is a limit value commonly used in the UPC regime. The saturation model is more suitable in the region below $x = 0.01$, and for the large-$x$ limit, there is still a need for a complete analytical treatment. However, the photon flux at $y = 4$ corresponds to photons with energy $\sim$84 GeV (for $J/\psi$), which are strongly suppressed in relation to photons with energy $\lesssim$0.2 GeV, meaning that possible corrections to the dipole formalism for higher values of $x$ would be suppressed by the photon flux.

The transverse overlap of the photon-meson wave function, which is dominant in relation to the longitudinal component in $Q \sim 0$, can be written as [34]

$$(\psi_V^*\psi_\gamma)_T = \hat{e}_f e\frac{N_c}{\pi z(1-z)}\{m_f^2K_0(\epsilon r)\phi_T(r,z) - [z^2+(1-z)^2]\epsilon K_1(\epsilon r)\partial_r\phi_T(r,z)\}, \quad (10)$$

where $\hat{e}_f = 1/3$ for $J/\psi$, $e = \sqrt{4\pi\alpha_{em}}$, $\epsilon^2 = z(1-z)Q^2 + m_f^2$, and $N_c = 3$. The phenomenological function $\phi_T(r,z)$ represents the scalar part of the meson wave function, and, here, we used the Boosted-Gaussian model [37], since it can be applied in a systematic way for the excited states, resulting in

$$\begin{aligned}\phi_{1S}(r,z) &= G_{1S}(r,z)\\ \phi_{2S}(r,z) &= G_{2S}(r,z)[1+\alpha_{2S,1}g_{2S}(r,z)]\\ \phi_{3S}(r,z) &= G_{3S}(r,z)\Bigg\{1+\alpha_{3S,1}g_{3S}(r,z)+\alpha_{3S,2}\\ &\quad\times\left[g_{3S}^2(r,z)+4\left(1-\frac{4z(1-z)r^2}{R_{3S}^2}\right)\right]\Bigg\},\end{aligned}$$

where

$$G_{nS}(r,z) = \mathcal{N}_{nS}z(1-z)\exp \times\left(-\frac{m_{c/b}^2\mathcal{R}_{nS}^2}{8z(1-z)}-\frac{2z(1-z)r^2}{R_{nS}^2}+\frac{m_{c/b}^2\mathcal{R}_{nS}^2}{2}\right)$$

and

$$g_{nS}(r,z) = 2 - m_{c/b}^2\mathcal{R}_{nS}^2 + \frac{m_{c/b}^2\mathcal{R}_{nS}^2}{4z(1-z)} - \frac{4z(1-z)r^2}{R_{nS}^2}.$$

The free parameters $\mathcal{R}_{nS}^2$, $\mathcal{N}_{nS}$, and $\alpha_{nS}$ are determined from normalization, the orthogonality conditions, and a fit to the experimental leptonic decay width (more details are found in Refs. [38,39], in which the parameters are calculated).

The next term in Eq. (9) is the cross section $\sigma_{\mathrm{dip}}^{\mathrm{nucleus}}(x,r)$, calculated via the Glauber model [40],

$$\sigma_{\mathrm{dip}}^{\mathrm{nucleus}}(x,r) = 2\int d^2b\left\{1-\exp\left[-\frac{1}{2}T_A(b)\sigma_{\mathrm{dip}}^{\mathrm{proton}}(x,r)\right]\right\}, \quad (11)$$

where the nuclear profile function, $T_A(b)$, is obtained from a two-parameter Fermi distribution for the nuclear density [41] and the dipole cross section, $\sigma_{\mathrm{dip}}^{\mathrm{proton}}(x,r)$, is

TABLE I. Comparison of results for the $d\sigma/dy$ using GBW and IIM models with the ALICE data for $J/\psi$ [18].

| $d\sigma/dy$ [$\mu$b] | 30%–50% | 50%–70% | 70%–90% |
|---|---|---|---|
| | Average rapidity distribution—Scenario 1 | | |
| GBW | 200 | 100 | 60 |
| IIM | 170 | 84 | 51 |
| ALICE data | $73 \pm 44^{+26}_{-27} \pm 10$ | $58 \pm 16^{+8}_{-10} \pm 8$ | $59 \pm 11^{+7}_{-10} \pm 8$ |

modeled from the Golec-Biernat and Wüsthoff (GBW) [42] and IIM [25] models, since both models presented good results in the ultraperipheral regime [6–8].

Considering the kinematical range $2.5 < y < 4.0$ and $p_T < 0.3$ GeV, we combine the usual photon flux [Eq. (6)] with the photoproduction cross section [Eq. (8)] to calculate the average rapidity distribution as described in Sec. II. To take into account the centrality range, the relation $c = b^2/4R_A$ is used, where $c$ corresponds to centrality. Integrating in the impact parameter for the centrality classes (30%–50%, 50%–70%, and 70%–90%), the results shown in Table I, which also presents the ALICE data, are obtained. We observe excellent agreement with the data in the more peripheral region. In contrast, as going to more central regions, our estimates overstimate the ALICE data, and therefore some correction with $b$ dependence is required, as will be developed in the next section.

## IV. EFFECTIVE PHOTON FLUX

To improve the calculations, the photon flux is modified following a procedure similar to the one carried out in Ref. [21], in which an effective photon flux was built as a function of the usual photon flux with two restrictions: (1) only photons that reach the geometrical region of the nuclei-target are considered, and (2) the photons that reach the overlap region are not considered. Consequently, the vector $\vec{b}_1$ that starts in the center of the flux emitter nuclei maps only the allowed region of the target nuclei (shaded region of the Fig. 2). In contrast with Ref. [21], we do not divide by a fixed region $\pi R_A^2$. Being interested in collisions with centrality that extends from 30% to 90%, it is required

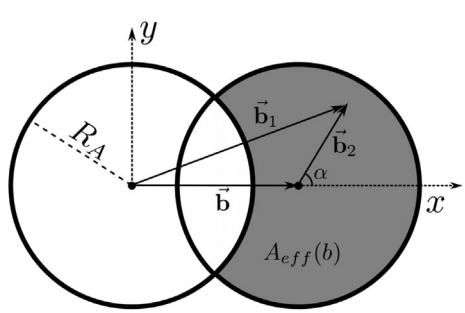


FIG. 2. Schematic drawing used in the construction of the effective photon flux.

to divide by the mapped areas, $A_{\rm eff}(b)$, enforcing $b$ dependence, thus obtaining

$$N^{\rm eff}(\omega,b) = \frac{1}{A_{\rm eff}(b)} \int d^2 b_1 N(\omega,b_1)\theta(R_A - b_2)\theta(b_1 - R_A), \tag{12}$$

where

$$A_{\rm eff}(b) = R_A^2\left[\pi - 2\cos^{-1}\left(\frac{b}{2R_A}\right)\right] + \frac{b}{2}\sqrt{4R_A^2 - b^2}.$$

The first condition to ensure that the effective photon flux refers only to photons that reach the geometrical region of the nuclei target is given by the function $\theta(R_A - b_2)$. Equation (12) can be correspondingly rewritten as

$$N^{\rm eff}(\omega,b) = \frac{1}{A_{\rm eff}(b)} \int b_2 db_2 d\alpha N(\omega,b_1)\theta(b_1 - R_A). \tag{13}$$

Here, the flux is expressed in terms of the new variable $(b_2,\alpha)$ related to $b_1$ through the equation $b_1^2 = b^2 + b_2^2 + 2bb_2\cos(\alpha)$. The $\theta(b_1 - R_A)$ function corresponds to the second condition and therefore discards the contribution of the photons that reach the overlap region where the nuclear effects are present. With this last condition, Eq. (13) can be separated in two components,

$$N^{\rm eff}(\omega,b) = \frac{1}{A_{\rm eff}(b)}[N^{\rm eff}_{\rm full}(\omega,b) - N^{\rm eff}_{\rm overlap}(\omega,b)]. \tag{14}$$

The first term, $N^{\rm eff}_{\rm full}(\omega,b)$, maps all the nuclear region, including the overlap region,

$$N^{\rm eff}_{\rm full}(\omega,b) = \int b_2 db_2 d\alpha N(\omega,b_1);$$

the second term, $N^{\rm eff}_{\rm overlap}$, maps only the overlap region, and its contribution is defined in the Cartesian coordinate system by

$$N^{\rm eff}_{\rm overlap}(\omega,b) = 2\int_0^{b_{y\,\rm max}} db_y \int_{b_{x\,\rm min}}^{b_{x\,\rm max}} db_x N(\omega,b_1), \tag{15}$$

where $b_1^2 = b_x^2 + b_y^2$ and the integration limits are $b_{x\,\rm min} = -\sqrt{R_A^2 - b_y^2} + b$, $b_{y\,\rm max} = \sqrt{R_A^2 - (\frac{b}{2})^2}$, and $b_{x\,\rm max} = \sqrt{R_A^2 - b_y^2}$. For purposes of numerical calculation, it is more useful to disconnect the dependence of the $b_{x\,\rm min}$ and $b_{x\,\rm max}$ with $b_y$. This is achieved with the change of variables $b_y = g_1(b)b_y'$ and $b_x = g_2(b,b_y)b_x' + b/2$, where the Jacobian functions $g_{1,2}$ are, respectively, given by

$g_1(b) = \sqrt{R_A^2 - (b/2)^2}$ and $g_2(b, b_y) = (\sqrt{R_A^2 - b_y^2} - b/2)$. In terms of the new variables, Eq. (15) can be rewritten as

$$N^{\rm eff}_{\rm overlap}(\omega, b) = 2\int_0^1 \int_{-1}^1 db'_y db'_x g_1(b) g_2(b, b_y) N(\omega, b_1). \tag{16}$$

Figure 3 presents the comparison of the usual photon flux [Eq. (6)] with the effective photon flux [Eq. (14)] for the energies $\omega = 0.01$ GeV and $\omega = 1$ GeV, since for the centrality class 30%–90% the photon flux is formed mainly for photons with energy $\omega < 200$ MeV. For $b \lesssim 4$ fm (centrality $\lesssim$8%), the usual photon flux considerably diverges from the effective photon flux, tending to 0 as $b \to 0$. Otherwise, in the range $4\ \text{fm} \lesssim b \lesssim 11$ fm ($8\% \lesssim$ centrality $\lesssim 60\%$), the usual photon flux is higher than the effective photon flux, mainly in the limit $b \sim R_A \sim 7$ fm. At last, in the region $b > 11$ fm, the two models become similar for the energy $\omega = 0.01$ GeV and $\omega = 1$ GeV, approaching each other as we reach the ultraperipheral regime ($b > 2R_A$).

Using the effective photon flux [Eq. (14)], the rapidity distribution is calculated for the nuclear photoproduction of the $J/\psi$ in Pb-Pb collisions at $\sqrt{s} = 2.76$ TeV and $\sqrt{s} = 5.02$ TeV. First, in Fig. 4, our estimates are given for the centrality classes 30%–50%, 50%–70%, and 70%–90% with $\sqrt{s} = 2.76$ TeV, using the GBW and IIM dipole models. Comparing both dipole models, there is some difference in the $|y| \gtrsim 1.0$ range, although the curves show similar behavior. The comparison between the different centrality classes can provide more interesting information on how far the adopted formalism can be extrapolated. Especially, we observed an increase of ~12% from 70%–90% to 50%–70% and of ~13.7% from 50%–70% to 30%–50%, for both dipole models, at $y = 0$. Similarly, at $\sqrt{s} = 5.02$ TeV, we observed an increase of ~12% from 70%–90% to 50%–70% and ~13.3% from 50%–70% to 30%–50% at $y = 0$, as shown in Fig. 5. Therefore, the relative variation between the different centrality classes is not sensitive to the increase of the energy.

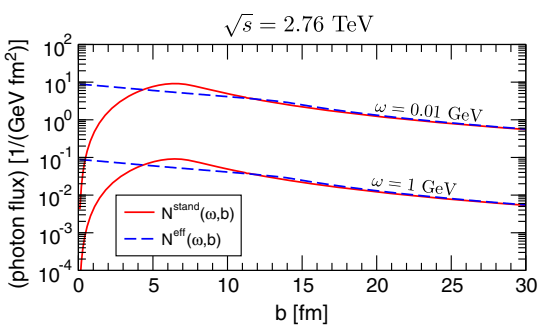


FIG. 3. Comparison between the usual photon flux (solid line) and the effective photon flux (dashed line) for the photon energy values $\omega = 0.01$ GeV and $\omega = 1$ GeV.

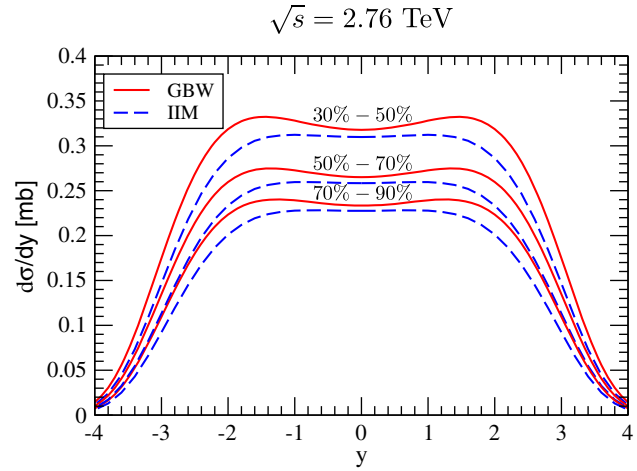


FIG. 4. Rapidity distribution for $J/\psi$ nuclear photoproduction at $\sqrt{s} = 2.76$ TeV for different centrality classes using the GBW and IIM dipole models.

The ratio $\frac{d\sigma^{5.02}}{dy} / \frac{d\sigma^{2.76}}{dy}$ was also analyzed, obtaining an increase of approximately 30% in the central rapidity region $|y| < 1.5$ for the three investigated centrality classes. This ratio is, approximately, 60% for the same rapidity region in the UPC. It can indicate that this formalism for the effective photon flux seems less sensitive with the variation of the energy in comparison to the usual photon flux.

To compare with ALICE measurements, the average rapidity distribution was recalculated in the $2.5 < y < 4.0$ range, using the effective photon flux without changing the photonuclear cross section (scenario 2), and the results are presented in Table II. Better agreement with the data in the central region is observed. Especially, the use of the IIM model produces better results than those produced by the GBW model.

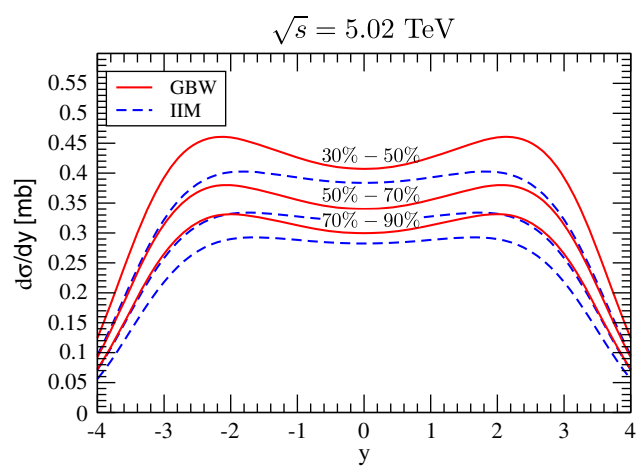


FIG. 5. Rapidity distribution for $J/\psi$ nuclear photoproduction at $\sqrt{s} = 5.02$ TeV for different centrality classes using the GBW and IIM dipole models.

TABLE II. Average rapidity distribution compared with ALICE data [18].

| $d\sigma/dy$ [$\mu$b] | 30%–50% | 50%–70% | 70%–90% |
|---|---|---|---|
| | Average rapidity distribution—Scenario 2 | | |
| GBW | 128 | 98 | 80 |
| IIM | 107 | 80 | 67 |
| ALICE data | $73 \pm 44^{+26}_{-27} \pm 10$ | $58 \pm 16^{+8}_{-10} \pm 8$ | $59 \pm 11^{+7}_{-10} \pm 8$ |

## V. EFFECTIVE PHOTONUCLEAR CROSS SECTION

Until now, the transition from the ultraperipheral to peripheral regime was performed by changing only the photon flux. However, knowing that in the build of the effective photon flux the nuclear overlap region was not considered, for consistency, it is also necessary to discard the photon-target interaction in the overlap region. With the restriction $\Theta(b_1 - R_A)$ in Eq. (11), only the interaction of the photon with the nonoverlap region is considered. Equation (11) can be written as

$$\sigma_{\rm dip}^{\rm nucleus}(x,r) = 2\int db d\alpha b \Theta(b_1 - R_A) \times \left\{1 - \exp\left[-\frac{1}{2}T_A(b)\sigma_{\rm dip}^{\rm proton}(x,r)\right]\right\},$$

TABLE III. Comparison of the results in the scenario 3 with the ALICE data [18].

| $d\sigma/dy$ [$\mu$b] | 30%–50% | 50%–70% | 70%–90% |
|---|---|---|---|
| | Average rapidity distribution—Scenario 3 | | |
| GBW | 73 | 78 | 75 |
| IIM | 61 | 66 | 63 |
| ALICE data | $73 \pm 44^{+26}_{-27} \pm 10$ | $58 \pm 16^{+8}_{-10} \pm 8$ | $59 \pm 11^{+7}_{-10} \pm 8$ |

where $b_1^2 = B^2 + b^2 + 2Bb\cos(\alpha)$, with $B$ the impact parameter of the nuclear collision. The combination of the modifications in the photon flux and in the photonuclear cross section constitutes scenario 3, which produces the results for the rapidity distribution presented in Table III.

For completeness, in addition to the $J/\psi$ state, the average rapidity distributions were also estimated for $\psi(2S)$ and for the three Υ states: $Y(1S)$, $Y(2S)$, and $Y(3S)$ with $\sqrt{s} = 5.02$ TeV. All the results are summarized in Table IV, where each pair of the values corresponds to the GBW (left) and IIM (right) models. It can be observed that the $Y(2S)$ and $Y(3S)$ are not good discriminators, since they produce similar results for the dipole models considered in the three scenarios. It can be observed that the relative variation between the scenarios is not dependent of the dipole models [for example, $(S_1/S_2)^{\rm GBW} \sim (S_1/S_2)^{\rm IIM}$] for each centrality class.

## VI. $R_{AA}$ RESULTS

Using Eq. (1), the nuclear modification factor, $R_{AA}$, was calculated for the three centrality classes investigated, considering the kinematic region $p_T < 0.3$ GeV/c and $2.5 < y < 4.0$. Using the IIM model, which gives better results, the three scenarios developed in this paper were compared with the ALICE data, as shown in Fig. 6. As can be observed, scenario 1 fits with the data only in the more peripheral region where the uncertainty is higher. However, in this scenario, no relevant modification was performed in relation to the ultraperipheral regime. For scenarios 2 and 3, where a deeper dependence with $b$ was applied, better results were achieved for the more central classes in which the uncertainty was small. It should be considered that the ALICE measurements, which depended on the centrality of the collision, were taken following the centrality criteria developed in Ref. [26], in which the ultraperipheral regime started in $b \sim 20$ fm, instead of the standard $b \sim 2R_A$. Consequently, the interval in $b$ corresponding

TABLE IV. Average rapidity distribution in the region $2.5 < y < 4.0$ for the mesons $\psi(2S)$ and $Y(1S, 2S, 3S)$ for the scenarios 1, 2, and labeled by S1, S2, and S3, respectively, presented as GBW/IIM.

| GBW/IIM | 30%–50% | 50%–70% | 70%–90% |
|---|---|---|---|
| $\psi(2S)$ ($\mu$b) | **S1**: 102.42/81.53 | **S1**: 53.92/43.20 | **S1**: 34.50/27.79 |
| | **S2**: 65.51/52.31 | **S2**: 51.32/41.05 | **S2**: 42.45/34.02 |
| | **S3**: 37.54/30.04 | **S3**: 41.24/33.08 | **S3**: 39.89/32.02 |
| $\Upsilon(1S)$ (nb) | **S1**: 425.35/398.00 | **S1**: 170.45/158.10 | **S1**: 88.16/80.70 |
| | **S2**: 247.7/230.86 | **S2**: 184.17/171.2 | **S2**: 144.45/133.87 |
| | **S3**: 142.70/133.02 | **S3**: 149.50/126.53 | **S3**: 136.50/126.53 |
| $\Upsilon(2S)$ (nb) | **S1**: 69.01/68.83 | **S1**: 26.85/26.43 | **S1**: 13.55/13.08 |
| | **S2**: 39.88/39.55 | **S2**: 29.51/29.17 | **S2**: 23.03/22.67 |
| | **S3**: 23.07/22.83 | **S3**: 24.08/23.75 | **S3**: 21.85/21.46 |
| $\Upsilon(3S)$ (nb) | **S1**: 32.92/33.50 | **S1**: 12.62/12.65 | **S1**: 6.29/6.17 |
| | **S2**: 18.95/19.17 | **S2**: 14.00/14.10 | **S2**: 10.90/10.93 |
| | **S3**: 10.95/11.07 | **S3**: 11.40/11.48 | **S3**: 10.32/10.35 |

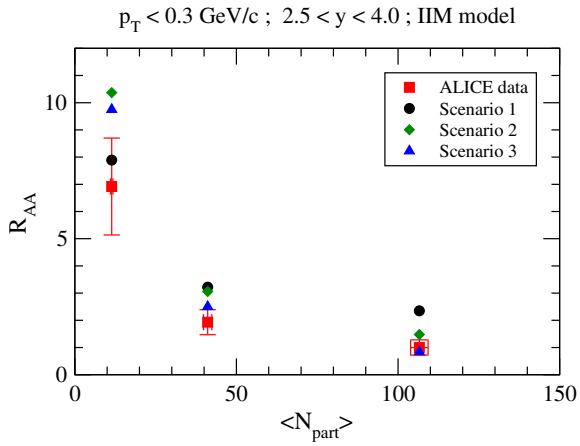


FIG. 6. Comparison of the $R_{AA}$ results with the ALICE data for the centrality classes 30%–50%, 50%–70% and 70%–90% [18].

to 70%–90%, for example, is not exactly the same as that obtained from the relation $c = b^2/4R_A$, employed in this work and closest to the Glauber model. This correction is required for a deeper comparison with the data, although main conclusions should not be affected.

## VII. SUMMARY

In this paper, we calculated the average rapidity distribution for the $V = (J/\psi, \psi(2S), \Upsilon(1S), \Upsilon(2S), \Upsilon(3S))$ mesons, and the nuclear modification factor for the $J/\Psi$ state in the centrality classes 30%–50%, 50%–70% and 70%–90% was estimated. The ALICE data were compared with our estimates, obtained from three different approaches. In the simplest approach (scenario 1), we obtained better agreement with the data only in the more peripheral region, where there is considerable uncertainty. For the more consistent approach (scenario 3), the result agrees better with the data in the more central region where the uncertainty is small. Although it is not yet possible to confirm that the exclusive photoproduction is fully responsible for the $J/\psi$ excess observed in ALICE, there are indications that it produces a considerable part of the effect.

## ACKNOWLEDGMENTS

We would like to thank Dr. Ionut Arsene for useful discussions. This work was partially financed by the Brazilian funding agency CNPq.

[1] M. Arneodo and M. Diehl, in Proceedings of the Workshop on HERA and the LHC, DESY and CERN, arXiv:hep-ph/0511047.
[2] M. G. Ryskin, A. D. Martin, and V. A. Khoze, Eur. Phys. J. C **54**, 199 (2008).
[3] D. d'Enterria, AIP Conf. Proc. **1038**, 95 (2008).
[4] M. Diehl, Phys. Rep. **388**, 41 (2003).
[5] I. P. Ivanov, N. N. Nikolaev, and A. A. Savin, Phys. Part. Nucl. **37**, 1 (2006).
[6] M. B. Gay Ducati, F. Kopp, M. V. T. Machado, and S. Martins, Phys. Rev. D **94**, 094023 (2016).
[7] M. B. Gay Ducati, M. T. Griep, and M. V. T. Machado, Phys. Rev. D **88**, 017504 (2013).
[8] G. S. dos Santos and M. V. T. Machado, J. Phys. G **42**, 105001 (2015).
[9] T. Lappi and H. Mantysaari, Phys. Rev. C **87**, 032201 (2013).
[10] V. Guzey, E. Kryshen, and M. Zhalov, Phys. Rev. C **93**, 055206 (2016).
[11] R. Fiore, L. Jenkovszky, V. Libov, M. V. T. Machado, and A. Salii, AIP Conf. Proc. **1654**, 090002 (2015).
[12] R. Fiore, L. Jenkovszky, V. Libov, and M. V. T. Machado, Theor. Math. Phys. **182**, 141 (2015).
[13] N. N. Nikolaev and B. G. Zakharov, Phys. Lett. B **332**, 184 (1994); Z. Phys. C **64**, 631 (1994).
[14] A. H. Mueller and J. W. Qiu, Nucl. Phys. **B268**, 427 (1986).
[15] L. N. Epele, C. A. Garcia Canal, and M. B. Gay Ducati, Phys. Lett. B **226**, 167 (1989).
[16] A. L. Ayala, M. B. Gay Ducati, and E. M. Levin, Nucl. Phys. **B493**, 305 (1997).
[17] A. L. Ayala, M. B. Gay Ducati, and E. M. Levin, Nucl. Phys. **B511**, 355 (1998).
[18] J. Adam *et al.* (ALICE Collaboration), Phys. Rev. Lett. **116**, 222301 (2016).
[19] W. Zha, J. Phys. Conf. Ser. **779**, 012039 (2017).
[20] M. B. Gay Ducati and S. Martins, Phys. Rev. D **96**, 056014 (2017).
[21] M. K. Gawenda and A. Szczurek, Phys. Rev. C **93**, 044912 (2016).
[22] W. Zha, S. R. Klein, R. Ma, L. Ruan, T. Todoroki, Z. Tang, Z. Xu, C. Yang, Q. Yang, and S. Yang, Phys. Rev. C **97**, 044910 (2018).
[23] J. G. Contreras, Phys. Rev. **C96**, 015203 (2017).
[24] E. Iancu, K. Itakura, and S. Munier, Phys. Lett. B **590**, 199 (2004).
[25] B. Abelev *et al.* (ALICE Collaboration), Phys. Lett. B **734**, 314 (2014).
[26] B. Abelev *et al.* (ALICE Collaboration), Phys. Rev. C **88**, 044909 (2013).
[27] B. Abelev *et al.* (ALICE Collaboration), Phys. Lett. B **718**, 295 (2012).
[28] C. A. Bertulani, S. R. Klein, and J. Nystrand, Annu. Rev. Nucl. Part. Sci. **55**, 271 (2005).
[29] F. Krauss, M. Greiner, and G. Soff, Prog. Part. Nucl. Phys. **39**, 503 (1997).
[30] K. T. R. Davies and J. R. Nix, Phys. Rev. C **14**, 1977 (1976).

[31] S. Klein and J. Nystrand, Phys. Rev. C **60**, 014903 (1999).
[32] A. Adeluyi and C. A. Bertulani, Phys. Rev. C **85**, 044904 (2012).
[33] V. P. Gonçalves and M. V. T. Machado, Eur. Phys. J. C **40**, 519 (2005).
[34] H. Kowalski, L. Motyka, and G. Watt, Phys. Rev. D **74**, 074016 (2006).
[35] A. G. Shuvaev, K. J. Golec-Biernat, A. D. Martin, and M. G. Ryskin, Phys. Rev. D **60**, 014015 (1999).
[36] M. L. Good and W. D. Walker, Phys. Rev. **120**, 1857 (1960).
[37] J. Nemchik, N. N. Nikolaev, E. Predazzi, and B. G. Zakharov, Z. Phys. C **75**, 71 (1997).
[38] N. Armesto and A. H. Rezaeian, Phys. Rev. D **90**, 054003 (2014).
[39] B. E. Cox, J. R. Forshaw, and R. Sandapen, J. High Energy Phys. 06 (2009) 034.
[40] N. Armesto, Eur. Phys. J. C **26**, 35 (2002).
[41] C. W. De Jager, H. De Vries, and C. De Vries, At. Data Nucl. Data Tables **14**, 479 (1974).
[42] K. Golec-Biernat and M. Wüsthoff, Phys. Rev. D **59**, 014017 (1998).